Paraexcitons of Cu_2O confined by a strain trap and high magnetic fields

Christian Sandfort, Jan Brandt,* Christoph Finke, Dietmar Fröhlich, and Manfred Bayer
Fakultät Physik, Technische Universität Dortmund, D-44221 Dortmund, Germany

Heinrich Stolz
Fachbereich Physik, Universität Rostock, D-18051 Rostock, Germany

Nobuko Naka
Department of Physics, Kyoto University, Kyoto 606-8502, Japan and
PRESTO, JST, 4-1-8 Honcho Kawaguchi, Saitama 332-0012, Japan

(Received 21 February 2011; revised manuscript received 6 October 2011; published 31 October 2011)

Spectrally and spatially resolved measurements of yellow 1*S* orthoexcitons and paraexcitons of Cu_2O in strain-induced traps are presented. Trap depths up to 31 meV for orthoexcitons and 23 meV for paraexcitons are achieved. In addition, a magnetic field up to 10 T is applied. With a theoretical model taking into account the strain- and magnetic-field-induced mixing of 1*S* yellow and green excitons, the experimental data of trap-depth-dependent and magnetic-field-dependent shifts can be explained. Furthermore, the polarization dependence of the emission of trapped paraexcitons is investigated. Spatially resolved, an intensity-dependent splitting of the luminescence polarized parallel to the symmetry axis of the strain trap is observed. Finally, phonon replica of trapped orthoexcitons and paraexcitons in a magnetic field are presented, which allow us to map a large range of exciton wave vectors.

DOI: 10.1103/PhysRevB.84.165215 PACS number(s): 78.20.−e, 71.35.Cc, 71.36.+c

I. INTRODUCTION

Cuprous oxide (Cu_2O) is still a hot candidate for Bose-Einstein condensation (BEC) of bulk excitons since there are recent theoretical claims[1,2] that BEC of paraexcitons manifests itself in distinct signatures of spatially resolved luminescence of excitons in a trap. For a review of earlier experiments, we refer to Ref. 3. Former attempts to create a BEC in Cu_2O failed due to the fast decay of excitons at high densities by Auger-type decay.[4–6] At lowest temperatures, the thermalization time of a paraexciton gas with the phonon bath increases due to the decreasing interaction with acoustic phonons.[7] Confining the excitons in a strain trap,[8–11] however, might help to overcome the obstacles of a fast decay by Auger-type processes. In this respect, an anomalous heating of the exciton gas in experiments similiar to those reported in this paper, albeit at sub-Kelvin bath temperatures, has been interpreted as an indication of the transition into a BEC.[12]

In order to investigate in detail the expected spatially resolved spectra of excitons in a strain trap, a special optical setup was designed. By use of a double monochromator in second order, a spectral resolution of 7 μeV and a spatial resolution of 6 μm were accomplished. A shallow depth of field and focus is achieved by telescopic imaging of the photoluminescence (PL). In order to study solely the spatial distribution of trapped excitons, the monochromator is set to zeroth order. The polarization of the paraexciton luminescence shows a pronounced spatial dependence. Trap depths up to 31 meV for orthoexcitons and 23 meV for paraexcitons are achieved. With an additional magnetic field up to 10 T, a red-shift of the paraexciton for different trap depths is observed. For paraexcitons, there is an increase of the red-shift up to a factor 5 as compared to the strain-free case. The magnetic field data for different trap depths are analyzed by taking into account the strain-induced interaction with green excitons.[13,14] The magnetic field causes a mixing of the paraexciton with the yellow orthoexciton, which leads to a further increase of the oscillator strength of the paraexciton[15] in addition to the strain-induced oscillator strength due to the mixing with green excitons. The magnetic-field-induced mixing with the yellow orthoexciton gives rise to strong phonon emission of the paraexciton,[16] which allows one to map a large range of exciton wave vectors down to $k = 0$ in contrast to the no-phonon quadrupole emission.

The paper is organized as follows. In Sec. II, the theory for the strain splitting and the additional red-shift of paraexcitons due to the magnetic field in Faraday configuration is presented. The experimental setup is discussed in detail in Sec. III followed by a presentation of the experimental results, their discussion (Sec. IV), and conclusions with an outlook on further experiments to create a Bose-Einstein condensate of bulk excitons (Sec. V).

II. THEORY

The yellow exciton series in Cu_2O results from holes in the upmost valence band of $^2\Gamma_7^+$ symmetry and electrons in the lowest conduction band of $^2\Gamma_6^+$ symmetry, which are separated by a band gap of 2.173 eV. The green series is shifted by spin-orbit splitting of the valence band ($^4\Gamma_8^+$ symmetry) by 131 meV to higher energy.[17] The exciton symmetries are derived from the corresponding band symmetries. For the yellow series, $^2\Gamma_7^+ \otimes {}^2\Gamma_6^+ = {}^1\Gamma_2^+ \oplus {}^3\Gamma_5^+$ leads to the spin-triplet paraexciton $^1\Gamma_2^+$ and singlet-triplet mixed orthoexciton ($^3\Gamma_5^+$), which is optically allowed for quadrupole transitions. The green excitons are derived from $^4\Gamma_8^+ \otimes {}^2\Gamma_6^+ = {}^2\Gamma_3^+ \oplus {}^3\Gamma_4^+ \oplus {}^3\Gamma_5^+$, where the twofold $^2\Gamma_3^+$ and the threefold $^3\Gamma_4^+$ refer to the paraexcitons and the threefold $^3\Gamma_5^+$ to the orthoexciton.

In the following, the mixing of yellow and green excitons for strained samples in a magnetic field is examined. Strain applied along [001] with a so-called Hertzian contact lowers the symmetry along the stress axis from O_h to D_{4h}. Due to parity, P excitons are not mixed with S excitons and, hence, only S excitons have to be considered.

With strain and external magnetic field, the effective Hamiltonian for excitons reads as

$$H = H_0 + H_{ex} + H_d + H_m. \tag{1}$$

The electron-hole exchange H_{ex} can be expressed by

$$H_{ex} = 2\, J_{mn}\, \mathbf{S}_e \cdot \mathbf{S}_h \tag{2}$$

with the exchange matrix elements J_{mn} and the operators

$$\mathbf{S}_{e,h} = \tfrac{1}{2}\sigma_{e,h}, \tag{3}$$

where $\sigma_{e,h}$ are the Pauli matrices. The electron-hole exchange splits the orthoexcitons from the paraexcitons [12.12 meV (Ref. 18) for the yellow $1S$ excitons]. Furthermore, the exchange interaction leads to a mixing of the yellow and the green exciton series.[17]

The deformation Hamiltonian H_d for crystals of O_h symmetry is given by[14]

$$H_d = a\,\mathrm{Tr}\,\tilde{\varepsilon} + 3b\,\varepsilon_{ii}\left(L_i^2 - \frac{1}{3}\mathbf{L}^2\right) - \sqrt{3}d\,\varepsilon_{ij}(L_iL_j + L_jL_i), \tag{4}$$

where ε_{ij} are components of the strain tensor $\tilde{\varepsilon}$, $a = -2.15$ eV, $b = -0.43$ eV, $d = 0.36$ eV are the deformation potentials, and L_i are the components of the angular momentum operator. The strain tensor is calculated from the compliance constants[19] and the stress tensor for the Hertzian contact geometry.[20,21]

H_d describes the mixing of the yellow and green exciton series in a perturbing strain field, which shifts the exciton energy levels and transfers quadrupole oscillator strength to the yellow $1S$ paraexciton. For uniaxial strain along [001], the yellow $1S$ excitons split as sketched in Fig. 1 and the yellow ${}^1\Gamma_2^+$ paraexciton is mixed with one of the two green ${}^2\Gamma_3^+$ paraexcitons, which are quadrupole allowed. The shifts of the energy levels due to inhomogeneous and anisotropic strain fields depend on the position in the sample yielding a potential trap for the yellow $1S$ paraexcitons and orthoexcitons.[11,22] The analytical solution of the strain field caused by the Hertzian contact has already been presented several times.[20,21] For applied pressures around 5 kbar, the observed shifts of the yellow $1S$ excitons are in the order of 10 meV. Figure 2 shows the calculated strain-induced paraexciton potential for stress along [001]. In the vicinity of the trap, the potential in the xy plane can be approximated by a parabolic potential along the stress axis z by a Morse potential as shown in the cross sections in Fig. 2. For the single-frequency laser used (bandwidth 5 neV), depending on the photon energy and the selected position of excitation on the crystal, a small region of absorption is expected. The excitation of the laser in the trap is marked exemplarily as a red solid line in the xy-plane cross section and as a red dot in the z cross section. Driven by the potential gradient, excitons drift[23,24] from these positions into the trap as indicated by the arrows and the dashed curves.

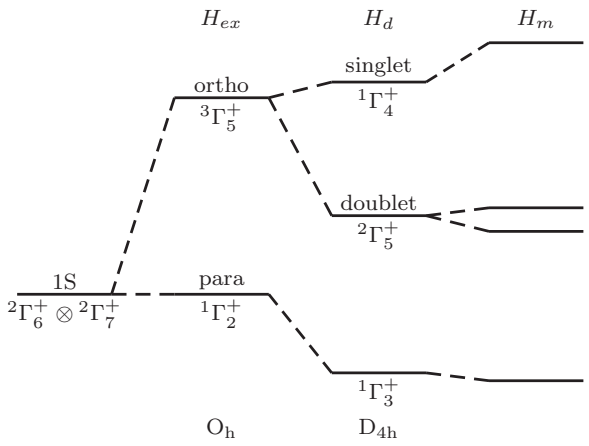

FIG. 1. Splitting of the yellow $1S$ excitons due to exchange interaction H_{ex}, uniaxial strain along [001] H_d, and magnetic field H_m along $[1\bar{1}0]$.

The magnetic field Hamiltonian is given by

$$H_m = -\frac{e\hbar}{2m_e} g_e \mathbf{B} \cdot \left(2\mathbf{S}_e - 2\frac{g_h}{g_e}\frac{m_e}{m_h}\mathbf{S}_h - \frac{g_h}{g_e}\frac{m_e}{m_h}\mathbf{L}\right) \tag{5}$$

with the effective masses $m_e = 0.99\,m_0$, $m_h = 0.58\,m_0$ of electron and hole[25] and their g factors.[18,26] Since the influence of the green series via the magnetic field interaction is small, the same g factor and mass are used for the ${}^4\Gamma_8^+$ and ${}^2\Gamma_7^+$ valence bands. In a magnetic field along $[1\bar{1}0]$, the degeneracy of the orthoexciton doublet is lifted along the strain axis and the paraexciton is mixed with the upper component.

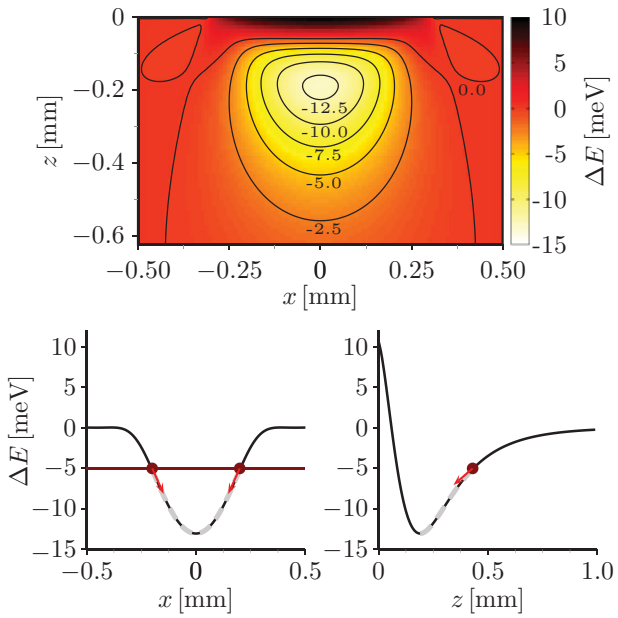

FIG. 2. (Color online) Calculated strain-induced paraexciton potential for strain applied along [001] with a lens radius of 7.78 mm and an applied pressure of 9.2 kbar. Upper panel: color-coded potential values ΔE with color code as indicated on right-hand side, and lines mark locations of equal strain-induced shifts in the plane of the trap minimum. Lower panel: cross section within the xy plane and along the stress axis z; red solid line and red dot mark the laser excitation; arrows and dashed curves indicate exciton filling of the trap.

Their repulsion shifts the paraexciton to lower energy and the orthoexciton state to higher energy. The lower component is shifted slightly toward lower energies (Fig. 1).

The shift due to strain is much larger than the shift due to a magnetic field ($\sim$70 μeV).[15] In order to calculate these shifts simultaneously, the strain and magnetic field Hamiltonian (1) is diagonalized numerically in the basis of the 1*S* yellow and the 1*S* green excitons. The 12 basis functions for the 1*S* excitons are taken from Ref. 13.

III. EXPERIMENTAL SETUP

An overview of the experimental setup is shown in Fig. 3. A single-frequency dye laser with a bandwidth of about 5 neV (Coherent 899-21) pumped by a solid-state laser (Coherent Verdi V-10) is used. The light passes a half-wave plate (WP_1) for setting the polarization of the incoming laser beam, which is then focused by a lens (L_1) on the crystal in the cryostat. For most of the measurements, a 10-T split-coil magneto-optic cryostat (Oxford Spectromag) is used. By use of two pumps (150 m^3/h and 60 m^3/h pump speed) for lowering the He pressure in the variable temperature insert of the cryostat, temperatures down to 1.25 K are achieved as measured with a calibrated Cernox (Lakeshore) temperature sensor.

For the application of inhomogeneous stress, an apparatus consisting of a glass lens (PL) with radius of curvature 7.78 or 4.65 mm is used that is pressed by a plunger P on the flat crystal surface. This Hertzian contact[20,21] leads to a point of highest stress a few tens to a few hundred micrometers below the contact plane. Special care is taken to center the lens on the crystal by use of a tightly fit plunger with the lens and an adjustable mask of 0.3 mm thickness below the crystal. As discussed in the previous chapter, for the stress axis along [001], the orthoexcitons split into a singlet shifted to higher energy and a doublet at lower energy. The paraexciton is shifted to lower energy.

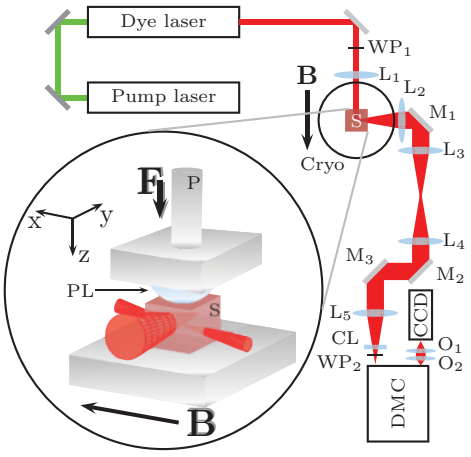

FIG. 3. (Color online) Schematic setup for spatially resolved spectra from a pressure-induced trap. CCD: charge-coupled device camera. CL: cylindrical lens. Cryo: magneto-optic cryostat. DMC: double monochromator. L_1 to L_5: lenses. M_1 to M_3: plane mirrors. P: plunger with pressure lens PL. S: Cu_2O sample. WP_1 and WP_2: half-wave plates. Force F applied along z, magnetic field along x; emission observed along y.

In order to resolve spatial patterns in the emission from the trap, the depth of field needs to be as small as possible. This is achieved by telescopic imaging of the sample with an aperture as large as possible (1:5 in our setup). As shown in Fig. 3, two lenses (L_3 and L_4) for an intermediate magnified image of the crystal are inserted. This has proven of value for alignment of the whole optical setup. It allows one to select emission from parts of the crystal with a precision adjustable cross slit and image it on the monochromator and to place a polarizer close to the intermediate image plane to analyze polarization effects. In the spectral range relevant for the experiments (610–625 nm in second order), the monochromator exhibits for horizontal polarization a four times higher transmission as compared to vertical polarization, whereas in zeroth-order, vertical polarization shows a four times higher transmission. Therefore, a half-wave plate (WP_2) is inserted in front of the monochromator in order to achieve the same conditions for both polarizations. Behind the monochromator, two high-quality photo objectives (O_1 and O_2) are placed for magnification by a factor 4. The sample is thus magnified by more than a factor 10 on the CCD camera. For most of the measurements, a CCD with a pixel size of 13.5 μm is used. The spectral resolution of the double monochromator (0.85 m Spex) in second order and a slit width of 40 μm is determined to be 7 μeV. In front of the monochromator, a cylindrical lens (CL, $f = 1$ m) is inserted for correction of astigmatism of the spherical mirrors in the monochromator. This correction is crucial for high-quality imaging as demonstrated in Fig. 4 by imaging of a 63-μm grid placed at the location of the sample. Without cylindrical lens, there is a perfect imaging only for the horizontal direction as expected for a monochromator with spherical mirrors. The grid is also used to determine the spatial calibration of the camera (μm/pixel). Once the setup is aligned for perfect telescopic imaging, only the first lens behind the cryostat (L_2) is adjusted for the final alignment. With this setup, the strain potential along the z axis is measured. In order to analyze the strain potential along the x axis, a periscope is inserted instead of the mirror M_2, which turns the image of the crystal on the entrance slit of the monochromator by 90°. An additional periscope has to be inserted to compensate for the

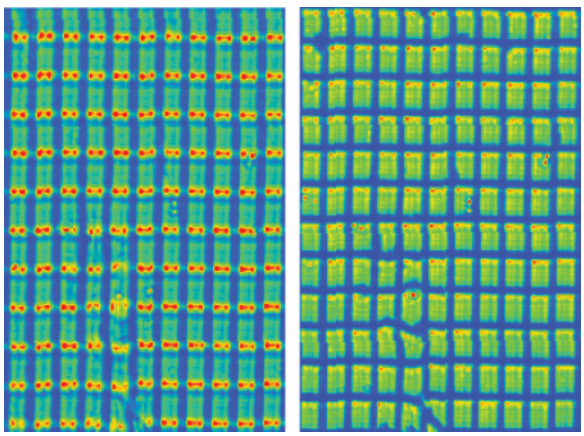

FIG. 4. (Color online) Images on CCD through monochromator (set to zeroth order) of 63-μm square grid, placed at the location of crystal. Left panel: without cylindrical lens for correction of astigmatism. Right panel: with cylindrical lens.

displacement in height. Since the mirror size of the periscopes does not allow us to catch the full aperture, two additional lenses (not shown in Fig. 3) have to be inserted to first cut down the cross section of the beam by about a factor 2 in front of the first periscope and then enlarge the cross section behind the second periscope by the same factor in order to achieve the same conditions for imaging on the entrance slit of the monochromator. For a perfect 90° turning of the crystal image on the entrance slit of the monochromator, a perfect 90° deflection of the second periscope is mandatory, which is verified by imaging the grid.

For most of the measurements, the crystal is excited along $[1\bar{1}0]$ and the emission is observed perpendicular to the excitation in [110]. Due to the high optical quality of the natural crystal used, there is no problem caused by scattered laser light. For observation along the direction of excitation $[1\bar{1}0]$, however, long pass filters have to be used for suppression of the intense laser light. For this configuration, an additional narrow band transmission filter for the pump laser is necessary in order to suppress the amplified spontaneous emission (ASE) of the dye laser.

IV. RESULTS AND DISCUSSION

In this section, the experimental results are presented and analyzed with use of the theory presented in Sec. II. Then, experimental results of the polarization and intensity dependence of the paraexciton emission are shown, which are measured in zeroth and second orders, making use of the insertion of a periscope in order to analyze the spectral dependence in the z direction (direction of applied stress). In addition, examples of phonon replica of orthoexciton and paraexciton spectra in the trap in a magnetic field are presented. Finally, the perspectives of these data on future experiments with the aim to observe BEC of trapped excitons in Cu_2O are discussed.

The externally applied pressure p_0 is an unaccessible parameter in the presented experiments. Nevertheless, the trap depths can be compared with theory by plotting the paraexciton trap energy ΔE_{para} as function of the orthoexciton trap energy ΔE_{ortho} for a given pressure p_0. This allows one to fit the model parameters to the data without knowledge of the applied pressure. In a second step, it is then possible to calculate the applied pressure from the measured shifts, although the accuracy of this indirect determination of the pressure is indefinite. Figure 5 shows the measured trap depths for different pressure settings and lens radii. Due to the high quality of the natural samples, trap depths up to 31 meV for the orthoexcitons and 23 meV for the paraexcitons are achieved. The solid line is obtained by solving the Hamiltonian (1) numerically. The dependence of the energy shift on the lens radius is negligible and, thus, both data sets can be fitted simultaneously with the exchange energies as fit parameters. For the exchange constants, $J_{yy} = J_{gg} = J_{yg} = -24.5$ meV is used, which slightly differ from that of Ref. 14. The analysis allows the determination of the external pressure as shown on the right-hand side.

In Fig. 6, experimental results of the magnetic field dependence of orthoexcitons and paraexcitons at different pressure settings and thus at different trap depths are presented.

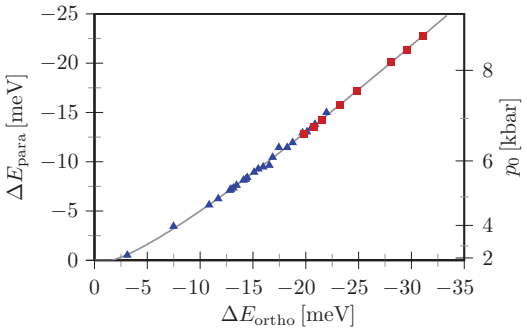

FIG. 5. (Color online) Plot of paraexciton trap depth (ΔE_{para}) as a function of orthoexciton trap depth (ΔE_{ortho}). Blue triangles: lens radius 7.78 mm. Red squares: lens radius 4.65 mm. Corresponding calculated pressure values are shown on the right side.

The model introduced in Sec. II is fitted to the data with use of the determined exchange parameters. Along the stress axis in a magnetic field, the doublet orthoexciton state splits and one state of the doublet shifts to lower energies, as is verified by the experiment (open circles and squares in Fig. 6). The other state of the doublet orthoexciton (dashed lines) shifts to higher energies due to its repulsion by the paraexciton. Experimentally, however, it can not be observed since its luminescence overlaps with the luminescence of the lower doublet state. With applied strain, there is an additional shift of the paraexciton trap minimum (filled circles and squares) to lower energies compared to the shift in a magnetic field in an unstrained crystal (filled pentagons). The numerical diagonalization of the strain and magnetic field Hamiltonian (1) shows additional shifts of the trap minima as shown by the two solid lines. Note that the model used neglects the mixing of the 1S green excitons with the 2S yellow excitons.[17] Nevertheless, this model already qualitatively explains the additional shift of the trap minima of the paraexciton in a magnetic field that arises mainly from the reduced energetic separation of the paraexciton and the upper doublet orthoexciton state as compared to the strain-free case. For visualization reasons, for the strain-free case, only the $M = 0$ orthoexciton is shown, which is not directly comparable to the doublet states in magnetic field. The excellent agreement of the theory with

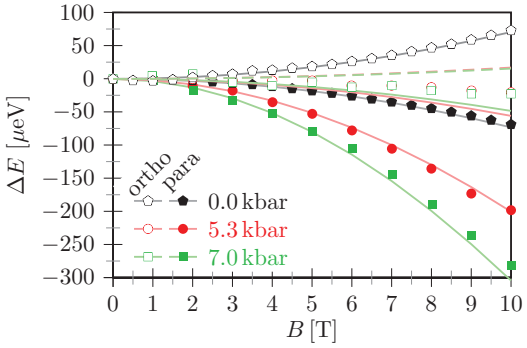

FIG. 6. (Color online) Magnetic field shift of paraexciton and orthoexciton in different strain potentials. Symbols: data points; lines: theory. The pressure p_0 is obtained from the shift of the trap depth (see Fig. 5).

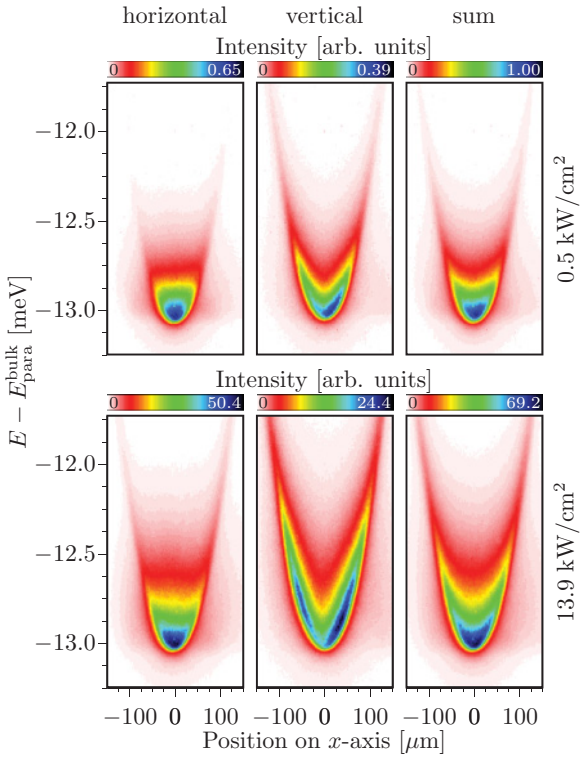

FIG. 7. (Color online) Polarization and intensity dependence of the paraexciton luminescence from the trap. Upper panel: 0.5 kW/cm^2. Lower panel: 13.9 kW/cm^2. Left panel: horizontal polarization. Middle panel: vertical polarization. Right panel: sum of both polarizations.

the experimental results is obtained by setting the g factors of the electron and the hole to $g_e = 1.7$, $g_h = 0$.

In the following, experimental results of the polarization and intensity dependence of the emission of paraexcitons in the trap are presented. As outlined in Sec. III, a periscope can be inserted in order to turn the image of the crystal on the entrance slit. This allows one to measure the spectral dependence of the luminescence (monochromator set to second order) for different positions along the x axis. Figure 7 shows the luminescence of the paraexciton in the trap along the x axis for horizontally and vertically polarized light and two different excitation intensities. Apparently, horizontally polarized light is observed primarily from the bottom of the trap (left panel), whereas vertically polarized light is mainly observed from excitons at higher energies and, thus, larger z positions (middle panel) that enter and populate the trap. This effect is most clearly seen if the excitation beam is close to the trap. As shown in Fig. 7, rather hot paraexcitons emit light with perpendicular polarization, whereas cold paraexcitons from the center of the trap radiate with horizontal polarization. One possible explanation is strain-induced birefringence as is observed for light passing through crossed polarizers. Such an effect, however, should depend strongly on the applied stress, which is not observed. Rather, we attribute the polarization effect to be caused by different selection rules due to lowering the symmetry outside the trap.

Along the main pressure axis [001], the point symmetry is D_{4h} and the Γ_2^+ paraexciton mixes with a Γ_3^+ green paraexciton state that is quadrupole allowed in horizontal polarization.[13,14,27] In the macroscopic 110 planes containing the plunger axis [001], the crystal locally retains its mirror symmetry across 110 and the paraexciton mixes with the same Γ_3^+ state as in the center of the trap, whereas in the macroscopic 100 planes containing the plunger axis, the compressive component along a ⟨010⟩ direction leads to mixing with a different Γ_3^+ state weakly radiating with vertical polarization. Furthermore, outside of the trap, the symmetry is reduced to D_{2h} and the paraexciton additionally mixes with a Γ_4^+ green orthoexciton state, which is magnetic dipole allowed emitting vertical polarization.[28] In general, radiation of vertical polarization is zero by symmetry in the macroscopic 110 planes containing the plunger axis, but is observable from other locations in the strain well. As the cloud of excitons becomes larger with increasing excitation intensity, the centroids of the vertically polarized luminescence spots move apart. We note that the intensity of a single polarization does not represent the true distribution of excitons in the trap. Also, the sum of the luminescence in both polarizations represents the distribution only after division by the radiative probability, which depends on the position in the trap, and one can obtain the exciton distribution.

Recently, it was suggested that luminescence might appear at high energies above the potential minimum when the paraexciton number in the trap rises above the critical number, which is proposed to be due to a competition of stimulated scattering of condensed excitons and inelastic scattering in the two-body decay.[12] Our observation of vertically polarized emission increasing with pump intensity might give another straightforward explanation of this effect.

In order to estimate the temperature of the excitons, the spectral and spatial distribution is fitted as in Refs. 9 and 29. For the low-intensity measurement shown in Fig. 7, a temperature of 1.4 K is obtained, whereas for the high intensity, 4.5 K is obtained. Hence, increasing the excitation intensity heats up the exciton system significantly.

In Fig. 8, emission spectra in zeroth order for horizontal and vertical polarized light are shown. For horizontally polarized light, there is only one spot observable, whereas for vertically polarized light, two spots are observed, which are displaced in the x direction (lower panel in Fig. 8). As shown in the upper panel in Fig. 8, the distance of these two spots depends on excitation intensity, and for low intensity in the vertical polarization, the distance of the two spots is so small that they can hardly be resolved.

As shown in the experimental setup (Fig. 3), the luminescence is detected perpendicularly to the exciting laser beam. In order to find out if the two horizontally displaced (right and left) spots are caused by the incoming and outgoing laser beams, respectively, we used the setup for observation of luminescence parallel to the exciting laser beam (see last paragraph of Sec. III). We again found two spots now displaced perpendicularly to the laser beam, which shows that the emission probability is maximal at this direction and thus substantiates the explanation given above.

Locally, the exciton wave vector has to be conserved[9] and, thus, the quadrupole emission from the trap samples only excitons with wave vectors $k = k_0$, which correspond to the wave vector of light at the given energy. As mentioned in the

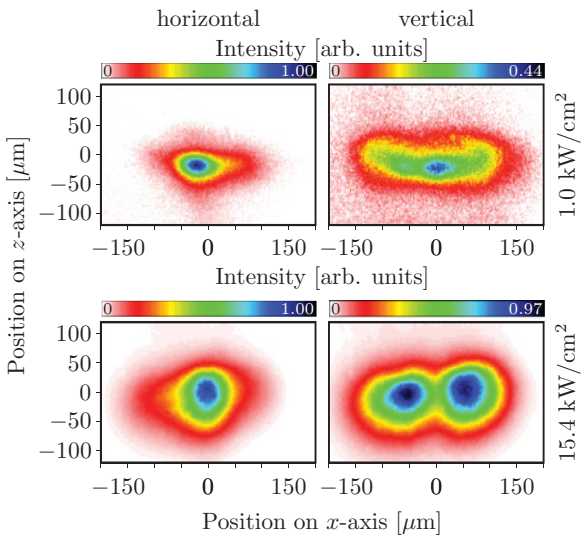

FIG. 8. (Color online) Two-dimensional images of the quadrupole emission of paraexcitons taken in the zeroth order of the monochromator for horizontal and vertical polarization and two different intensities; a narrow band filter in front of the monochromator selects only luminescence from the paraexciton trap; maximum intensity in the upper panel is 30% of that in the lower panel.

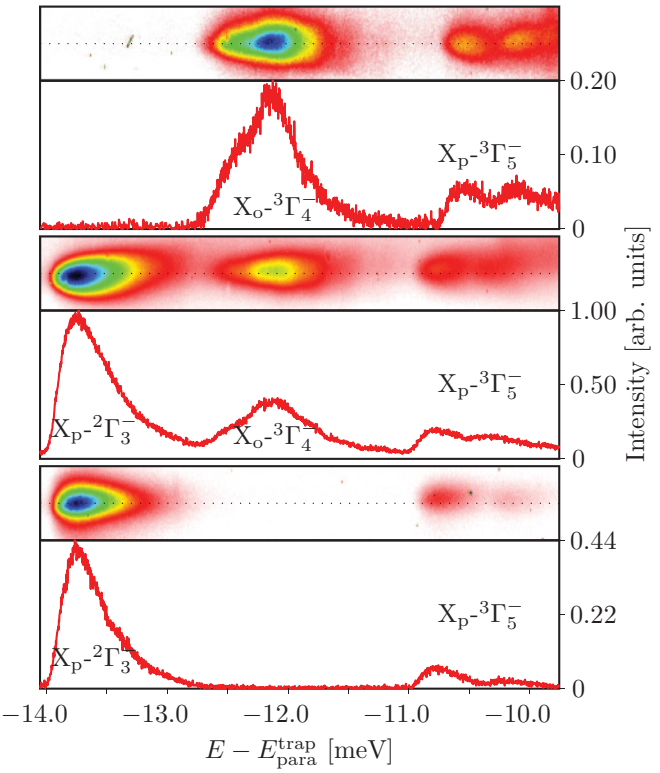

FIG. 9. (Color online) Spatially resolved phonon replica of trapped orthoexcitons ($^3\Gamma_4^-$ phonon) and trapped paraexcitons ($^2\Gamma_3^-$ and $^3\Gamma_5^-$ phonons) along the z axis in a magnetic field of 10 T. Two upper panels: pump laser energy 10.86 meV above trapped orthoexciton without (upper panel) and with magnetic field (middle panel). Lower panel: pump laser energy 0.77 meV above trapped paraexciton; spectra of the pixel row of maximum signal are shown below the corresponding spectral images.

Introduction, optical phonon replicas of the paraexciton are of special interest since they allow us to map the k distribution of the excitons. In Fig. 9, spatially resolved spectra for pumping above the orthoexciton resonance in the trap (upper panel) and close to the paraexciton resonance in the trap are presented. Below each spatially resolved spectrum, a spectrum for the pixel row of maximum signal is shown. Measurements in a magnetic field are very helpful since a strong emission of a $^2\Gamma_3^-$ phonon is found as compared to the rather weak $^3\Gamma_5^-$-phonon emission[16] as shown in the middle panel for excitation above the orthoexciton trap and in the lower panel for excitation less than 1 meV above the paraexciton trap. As expected, without magnetic field, the $^2\Gamma_3^-$-phonon emission disappears (upper panel). For excitation above the energy of the trapped orthoexciton (upper two panels), the $^3\Gamma_4^-$-phonon emission to the orthoexciton is clearly resolved. There is an indication of a splitting into transverse and longitudinal optical phonons.[16]

As expected, the threefold $^3\Gamma_5^-$ phonon (O_h symmetry without strain) splits in a strain field (D_{4h} symmetry) into two components. Resonant excitation of trapped paraexcitons should lead to ultracold excitons. Because of the confinement in the trap, the effective region of resonant absorption has only a length of a few micrometers, and it is probably not possible to reach densities above the critical density for BEC for the intensity of the cw laser used. A more efficient excitation might be to use the dipole-allowed anti-Stokes $^2\Gamma_3^-$-phonon absorption to the paraexciton in a magnetic field. The required shift of the laser energy of >13.6 meV is not transferred to the excitons, but used for emission of an optical phonon. For condensation into the lowest energy states at $k = 0$, additional relaxation processes by acoustic phonon emission and/or exciton-exciton scattering would be necessary; the cooling times are expected to be in the range of a few nanoseconds to a few tens of nanoseconds.[7,30,31] If the critical density for BEC is reached, it might show up as a characteristic low-energy peak in the phonon spectrum, indicative of a coherent population at $k = 0$, if phonon emission from the condensate occurs with sufficiently high probability as compared to the emission from the noncondensate fraction of the excitons in the trap.

V. CONCLUSIONS

With a setup allowing high spectral as well as spatial resolution, orthoexciton and paraexciton clouds in Cu_2O in a trap are studied. Trap depths up to 31 meV for orthoexcitons and 23 meV for paraexcitons are achieved. With a theoretical model, taking into account the mixing of yellow and green excitons for strained samples in a magnetic field, the pressure dependence of the trap depth and also the magnetic field dependence of orthoexcitons and paraexcitons can be described quantitatively. A pronounced polarization dependence of the paraexciton emission is observed. For vertical polarization, two horizontally displaced maxima are seen, the separation of which shrinks with decreasing pump intensity. Their spectral dependence is measured with a modified optical setup by which the image of the crystal on the entrance slit of the monochromator is turned by 90°. The polarization dependence is qualitatively explained by assuming strain-induced, spatially

dependent selection rules. Finally, phonon replica of orthoexcitons and paraexcitons in the trap are presented. Applying a magnetic field, the $^2\Gamma_3^-$-phonon replica of the paraexciton gets allowed. It is much more intense than the $^3\Gamma_5^-$ phonon and thus potentially well suited to study the exciton distribution down to $k = 0$. An intensity- and temperature-dependent low-energy structure might show up as a fingerprint of BEC. With the intensities of the cw laser used, it was not possible to observe such a structure. With a pulsed laser, one could increase the pump intensity by a factor of 1000. It is then a question as to whether the onset of Auger-type processes might allow us to go beyond the critical density for our lowest temperature of about 1.2 K. Time-resolved experiments are also necessary to study any high-energy features coming up with increasing intensity and distinguish them from hot excitons entering the trap.

ACKNOWLEDGMENT

We acknowledge the support by the Deutsche Forschungsgemeinschaft (SFB 651 "Starke Korrelationen im Strahlungsfeld" and "BA1549/18-1") and by KAKENHI (Grants No. 21740227 and No. 20104002) of MEXT, Japan.

*jan.brandt@tu-dortmund.de

[1] H. Stolz and D. Semkat, Phys. Rev. B **81**, 081302 (2010).
[2] S. Sobkowiak, D. Semkat, H. Stolz, T. Koch, and H. Fehske, Phys. Rev. B **82**, 064505 (2010).
[3] J. P. Wolfe, J. L. Lin, and D. W. Snoke, *Bose-Einstein Condensation of a Nearly Ideal Gas: Excitons in Cu_2O* (Cambridge University Press, Cambridge, UK, 1995), Chap. 13, p. 281.
[4] J. T. Warren, K. E. O'Hara, and J. P. Wolfe, Phys. Rev. B **61**, 8215 (2000).
[5] J. I. Jang and J. P. Wolfe, Phys. Rev. B **74**, 045211 (2006).
[6] K. Yoshioka, T. Ideguchi, A. Mysyrowicz, and M. Kuwata-Gonokami, Phys. Rev. B **82**, 041201 (2010).
[7] J. Brandt, P. Felbier, D. Fröhlich, C. Sandfort, M. Bayer, and H. Stolz, Phys. Rev. B **81**, 155214 (2010).
[8] D. P. Trauernicht, A. Mysyrowicz, and J. P. Wolfe, Phys. Rev. B **28**, 3590 (1983).
[9] D. P. Trauernicht, J. P. Wolfe, and A. Mysyrowicz, Phys. Rev. B **34**, 2561 (1986).
[10] N. Naka and N. Nagasawa, Phys. Rev. B **65**, 245203 (2002).
[11] N. Naka and N. Nagasawa, Phys. Rev. B **70**, 155205 (2004).
[12] K. Yoshioka, E. Chae, and M. Kuwata-Gonokami, Nat. Commun. **2**, 328 (2011).
[13] R. G. Waters, F. H. Pollak, R. H. Bruce, and H. Z. Cummins, Phys. Rev. B **21**, 1665 (1980).
[14] H. R. Trebin, H. Z. Cummins, and J. L. Birman, Phys. Rev. B **23**, 597 (1981).
[15] J. Brandt, D. Fröhlich, C. Sandfort, M. Bayer, H. Stolz, and N. Naka, Phys. Rev. Lett. **99**, 217403 (2007).
[16] C. Sandfort, J. Brandt, D. Fröhlich, M. Bayer, and H. Stolz, Phys. Rev. B **78**, 045201 (2008).
[17] C. Uihlein, D. Fröhlich, and R. Kenklies, Phys. Rev. B **23**, 2731 (1981).
[18] G. Baldassarri Höger von Högersthal, G. Dasbach, D. Fröhlich, M. Kulka, H. Stolz, and M. Bayer, J. Lumin. **112**, 25 (2005).
[19] M. H. Manghnani, W. S. Brower, and H. S. Parker, Phys. Status Solidi A **25**, 69 (1974).
[20] H. Hertz, J. Reine Angew. Math. **92**, 156 (1882).
[21] M. T. Huber, Ann. Phys. (NY) **319**, 153 (1904).
[22] D. W. Snoke and V. Negoita, Phys. Rev. B **61**, 2904 (2000).
[23] M. A. Tamor and J. P. Wolfe, Phys. Rev. Lett. **44**, 1703 (1980).
[24] D. P. Trauernicht and J. P. Wolfe, Phys. Rev. B **33**, 8506 (1986).
[25] T. Ohyama, T. Ogawa, and H. Nakata, Phys. Rev. B **56**, 3871 (1997).
[26] D. Fröhlich and R. Kenklies, Phys. Status Solidi B **111**, 247 (1982).
[27] K. E. O'Hara, Ph.D. thesis, University of Illinois, 1999.
[28] F. I. Kreingol'd and V. L. Makarov, Fiz. Tekh. Poluprovodn. **8**, 1475 (1974) [Sov. Phys. Semicond. **8**, 962 (1975)].
[29] R. Schwartz, N. Naka, F. Kieseling, and H. Stolz (submitted to New J. Phys.).
[30] A. L. Ivanov, C. Ell, and H. Haug, Phys. Rev. E **55**, 6363 (1997).
[31] C. Ell, A. L. Ivanov, and H. Haug, Phys. Rev. B **57**, 9663 (1998).